Ion energy distributions for collisional ion sheaths at an rf-biased plasma electrode

Xueying Victor Qin

Department of Electrical and Computer Engineering, University of Wisconsin-Madison

Abstract. In plasma etching for materials processing, ions are often accelerated towards the substrate via a sheath electric field generated by a bias voltage applied to the substrate electrode. By applying at tailored bias waveform to the electrode the resulting ion energy distribution can be manipulated to have a single narrow peak at a specified energy. For low neutral pressures, ion motion through the sheath is collisionless, and nearly all the incident ions strike the substrate with the full ion energy dictated by the bias waveform. However, as the plasma conditions are adjusted and the sheath thickness becomes long compared to the ion mean free path, the sheath becomes collisional. As ions undergo charge-transfer collisions while traversing the sheath, they strike the substrate with a lower ion energy than dictated by the bias waveform. As the system becomes more collisional, the peak of the ion energy distribution is suppressed, and the ion flux of lower-energy ions increases. Ion energy distributions at the substrate are measured with a retarding field energy analyzer for many systems of various collisionality, and the aforementioned effects of the collisional sheaths are observed.

1. Introduction

In plasma etching for semiconductor manufacturing, the average energy of ions striking the substrate can be controlled by applying an RF voltage to the substrate electrode. Because energetic ion bombardment of the substrate plays a role in producing high etch rates[1], selective etching, and vertical sidewalls, being able to selectively control the incident ion energy is of great importance. The voltage drop over the sheath next to the substrate is produced by the applied RF bias. Ions are accelerated by the electric field present within the sheath and strike the substrate. If the ions do not undergo any collisions during sheath traversal, they will strike the substrate at normal incidence and with ion energy equivalent to the sheath voltage drop.

If a sinusoidal RF bias voltage is applied to the substrate electrode, the peak-to-peak amplitude of the sinusoidal waveform determines the average incident ion energy. For the RF frequencies typically used for sinusoidal bias waveforms, the resulting ion energy distribution (IED) possesses two peaks at energy levels above and below the average bias voltage, with a span of intermediate energies. As the waveform frequency is increased, the "bimodal" distribution narrows and the peaks converge towards the average bias voltage. While increasing the waveform frequency does allow for a narrower IED, complications arise at very high frequencies due to standing waves across the electrode as the bias waveform wavelength becomes comparable to the electrode size. Because of this, the use of alternate bias waveform shapes has been developed in order to provide enhanced IED shape control without the complications arising from high-frequency sinusoidal biases. The results presented here consist of IEDs measured at the substrate, produced with a tailored bias waveform designed to generate single-peaked IEDs with the ability to control the energy and relative flux of the ion energy peak.

In this system an inductive RF power input controls the ion flux in the system while a tailored bias waveform applied to the substrate electrode controls the IED shape. The tailored bias waveform is an RF waveform composed of on the order of 10 harmonics of the fundamental frequency ($\approx$ 500 KHz in this case) while the amplitude and phase of the harmonics are adjusted to produce the desired waveform shape. An example of this single-level tailored bias waveform can be seen in Figure 1, consisting of a long period of constant voltage combined with a voltage spike, designed to produce a narrow IED. This produces a near constant sheath voltage aside from the duration of the spikes, resulting in nearly all incident ions acquiring approximately the same energy in the sheath. Assuming an absence of collisions in the sheath, the peak of the IED occurs at an energy corresponding to the constant voltage level, established by externally setting the height of the voltage spike.

To better understand the effects that collisions in the sheath can have on incident ion energies, it is necessary to measure the IEDs produced by collisional sheaths. To accomplish this, a range of plasma conditions must be produced, resulting in sheaths ranging from very collisionless to very collisional. The collisionality C of a given sheath can be defined as the ratio of the sheath thickness d_s to the mean free path λ_i, that is: $C = d_s/\lambda_i$. The mean free path is calculated from $\lambda_i = 1/n_n\sigma_i$, where n_n is the neutral argon gas density, and σ_i is the published argon-argon charge-transfer collision cross-sections[2]. While there exist cross-section values for momentum-transfer collisions, it is assumed the dominant interaction in the sheath is the charge-transfer collision[3]. If the sheath voltage V_s and ion current density J_i are known, the sheath thickness can be calculated in one of two ways: 1) for sheaths estimated to be in the collisionless regime, the sheath thickness is given by the Child-Langmuir Law:

$$d_s = \frac{2}{3}\left(\frac{2e}{m_i}\right)^{1/4}\left(\frac{\epsilon_0}{J_i}\right)^{1/2}\bar{V_s}^{3/4}. \tag{1}$$

For collisional sheaths, the sheath thickness is calculated from [4]:

$$d_s = \left(\frac{2e\lambda_i}{\pi m_i}\right)^{1/5}\left(\frac{2\epsilon_0}{3J_i}\right)^{2/5}\left(\frac{5}{3}\bar{V_s}\right)^{3/5}. \tag{2}$$

While the Child-Langmuir sheath calculation is intended for collisionless sheaths, we find that for a highly collisional case of 900 W RF power, 80 mTorr neutral pressure, and 300 V bias voltage, the sheath thicknesses calculated with each model are very similar. The Child-Langmuir Law gives d_s = 4.24E-3 m, while the collisional sheath thickness calculation gives d_s = 4.27E-3 m. If we use the Child-Langmuir sheath thickness the collisionality of this system is 3.17, near the upper end of the collisionality range explored in this experiment. However, the difference in sheath thickness is less than 1 percent. Additionally, it is difficult to specify a precise value of collisionality where the calculation of the sheath thickness should switch from the collisionless equation to the collisional equation. Because of this lack of a specific turning point and the similarity in sheath thickness calculations at high collisionality, as well as the validity of the Child-Langmuir sheath calculation at low collisionality, all sheath thicknesses used in this report will be calculated with the Child-Langmuir Law.

Given known values for argon-argon charge-transfer collision cross-sections at specific ion energies, through linear extrapolation the cross-sections for intermediate ion energies can be estimated. For a sheath voltages of 20V, σ_i = 4.5E-19 m^{-2}, while at a sheath voltage of 300V, σ_i = 3.6E-19 m^{-2}. The variation in σ_i for the range of ion energies investigated in this experiment is small: a 15x increase in the sheath voltage produces roughly a 25 percent decrease in the cross-section value. Alternatively, a change in the neutral pressure corresponds to a one-to-one change in the neutral density. In this experiment, the pressure varies in a range from 10 to 80 mTorr, and produces a corresponding effect on λ_i, leading to the conclusion that increasing neutral pressure is the most effective way to generate shorter mean free paths. Care must be taken to prevent J_i from becoming too low, causing baseline ion flux fluctuations to become more significant with respect to the peak ion flux and making peak identification difficult. In order to avoid this, the RF power can be increased to offset lowered ion current density, and larger sheath voltages will result in sheath thickness increasing at a greater rate than the ion mean free path (due to the low effect of ion energy on collisional cross section. Therefore, given the experiment's parameter space, to achieve high collisionality requires the use of high neutral pressure combined with a high RF power and sheath voltage. Conversely, low collisionality is most easily achieved at low neutral pressures.

For C less than 1, the sheath thickness is long compared to the ion mean free path and the sheath can be considered collisionless. For C greater than 1, the sheath thickness becomes comparable to or less than the ion mean free path, and the probability of ion charge transfer collisions in the sheath increase. These collisions that result in charge transfer will also serve to reduce the energy of the ion that ultimately bombards the substrate. This will affect the IED in two ways: 1) the peak height at the desired ion energy will be reduced, as the flux of full-energy ions arriving through the sheath decreases, and 2) there will be an increase in the flux of lower energy ions in the IED. In order to express this peak suppression, another parameter must be introduced. The area ratio AR is defined by:

$$AR = \frac{A_{peak}}{A_{total}}, \tag{3}$$

where A_{peak} is the mathematical area of the IED peak and A_{total} is the total area of the IED. Therefore the AR represents the fraction of incident ions that arrive with the intended energy of the peak. Since the AR is a normalized quantity, a consistent comparison can be made of IEDs obtained from a wide range of plasma conditions. It should be expected that for systems with similar collisionality, their IEDs should possess a similar AR. As collisionality increases, the resulting peak suppression should result in a decrease in AR.

2. Experimental Setup

All ion energy measurements were conducted in an argon helicon plasma. The substrate bias power supply consists of an arbitrary waveform generator and a broadband RF power amplifier (models ENI A500 and ENI A1000, 300 kHz - 35 MHz) connected via a blocking capacitor to the substrate electrode. This power supply is used to produce both sinusoidal and tailored bias voltage wave forms at the electrode. An electrically floating retarding field energy analyzer (RFEA), manufactured by Impedans® is integrated in the center of

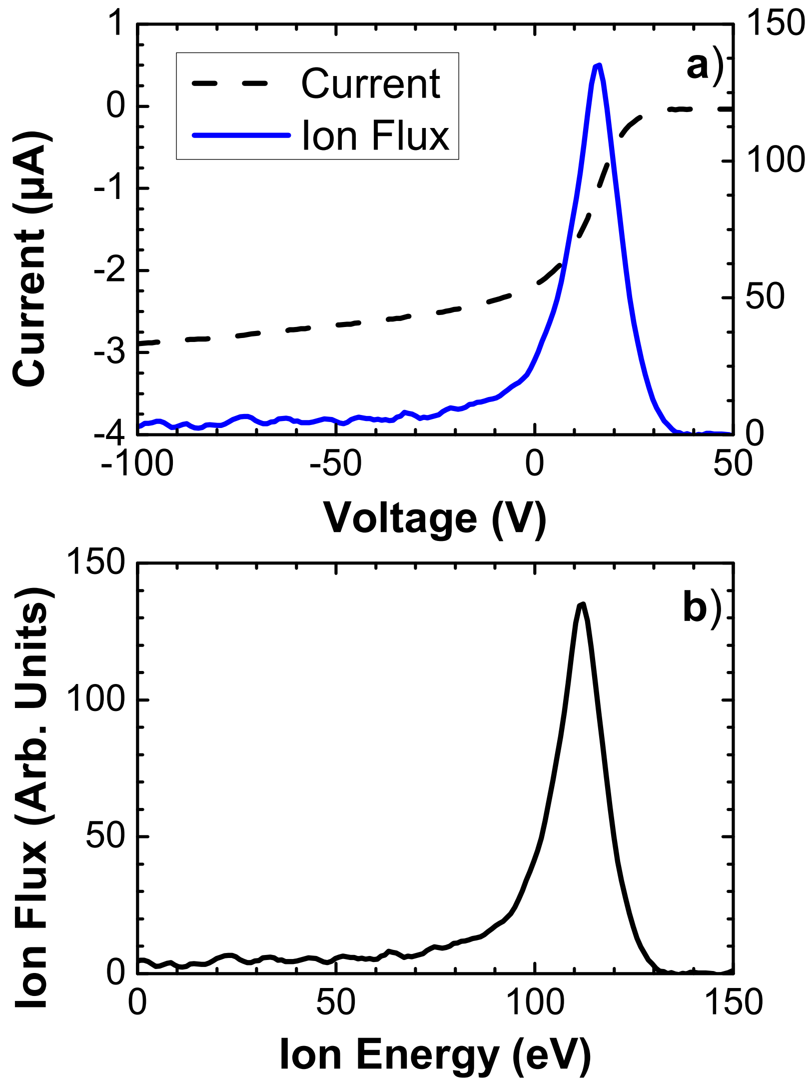

Figure 1. a) An example raw data trace measured with the RFEA for a single-peaked tailored waveform at 96 V. The ion current (dashed line) is measured by the collector grid, and the derivative of the curve is taken to obtain the ion flux (solid line). b) By shifting the horizontal axis by the average electrode voltage, the bias voltage scale becomes the ion energy scale and the ion energy distribution is obtained.

an aluminum disk 180 mm in diameter[5], matched to the electrode diameter. The disk is mechanically clamped on the electrode (in place of silicon wafers used in plasma processing experiments), allowing the disk to be electrically coupled to the electrode and biased at the same potential as the electrode. The gas mixture used for the ion energy measurements

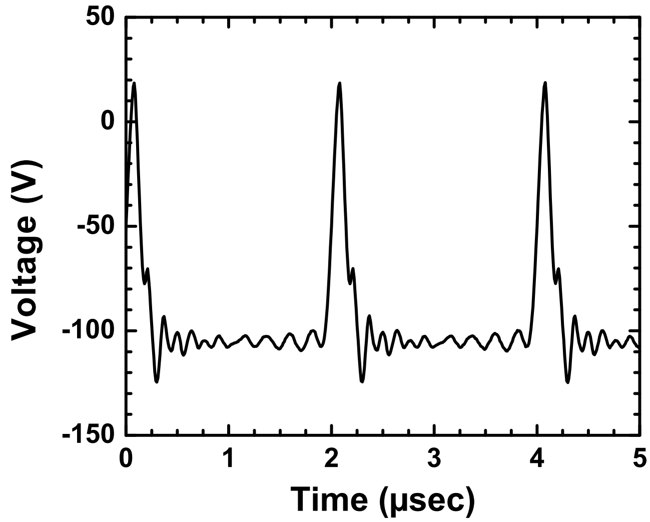

Figure 2. A tailored waveform with a single voltage level at approximately 100 V corresponding to the RFEA data in Figure 1, designed to produce an IED with a single narrow peak at near 100 eV.

contains 50 sccm Ar. An additional 7 sccm of He is introduced to the plasma through the electrode behind the RFEA disk to enhance heat transfer to the water-cooled electrode, with chilled water set at 5°C. The operating pressure and helicon RF power (13.56 MHz) for plasma production were varied to produce varying plasma conditions and collisionalities in the sheath. Pressures ranged from 10 mTorr to 80 mTorr, and the helicon RF power ranged from 300 W to 900 W. The chamber walls were heated to 90°C, a practice developed to maintain a constant wall temperature during plasma etching. The ion current density to the biased electrode is calculated from the measured time dependence of the blocking capacitor (capacitance $C_b = 3.29\ nF$) voltage. During periods of constant negative electrode voltage when the tailored waveform is applied, the capacitor is charged by the time-invariant ion current at the electrode, so that the capacitor voltage increases at a constant rate. The electrode current is then determined using the relation $I = C_b\, \mathrm{d}V/\mathrm{d}t$. The current density at the electrode is calculated by dividing the total electrode current by the electrode area, and was found to have values ranging from 0.3 to 18.9 $A\ m^{-2}$ for the conditions examined.

The RFEA is designed to measure the current of positive ions above a selected energy entering the analyzer. The analyzer contains a total of 3 parallel nickel mesh (50% transparency) grids in front of a nickel collector cut from a solid sheet, the ion current to which is recorded. The outermost grid (G1) is at the entrance of the analyzer facing the plasma, and is connected to the analyzer housing and is thus at the same potential as the biased electrode. G1 serves as the reference for dc voltages applied to the remaining grids. The second outermost grid (G2) is connected to the electron suppression voltage, which is maintained at a voltage level of -90 V relative to the average electrode bias. This grid serves to repel plasma electrons that enter the analyzer. The innermost grid (G3) is the selector grid to discriminate ions with different energies, swept over a specified voltage range. The instantaneous applied voltage on G3 sets the height of the potential barrier to prevent ions with insufficient energy from reaching the collector. This voltage range spans from below the G2 voltage to well above the DC plasma potential. The energy analyzer is designed so that each grid has a high impedance to ground over the range of frequencies applied to the electrode. There is also a high RF impedance (and low impedance at low frequency) to the DC voltage supplies used to bias the grids. This configuration, combined with a high capacitance between the grids, ensures that all grids follow the RF bias voltage applied to the electrode, so that the DC selector voltage applied to G3 is solely responsible for setting the height of the ion energy barrier. Sweeps of the selector voltage on G3 are conducted with a 1 V step size from negative to positive voltage across the sweep range. The collector (C) is a distance 0.6 mm from the entrance (G1) of the RFEA and is biased at -40 V relative to G1. Because this distance is considerably less than the ion mean free path over the parameter range studied, ion collisions within the analyzer are not expected to affect the measurements. The derivative of the collector current with respect to the selector voltage, proportional to ion flux to the RFEA at the associated energy is computed to produce the IED curve. An example of the collector current versus selector voltage and its derivative can be seen in Figure 1 for the electrode waveform shown in Figure 2. Since the selector grid voltage is referenced to the average electrode voltage, the IED is produced by replotting the derivative curve against ion energy by subtracting the average electrode voltage from the selector voltage values.

3. Results and Discussion

IEDs were measured for single-level tailored waveforms at various combinations of neutral pressure, RF power, and bias voltage level. Data was collected at neutral pressures of 10, 40, 60, 70, and 80 mTorr, RF power levels of 300, 600, and 900 W, and bias voltages of 20, 100, 200, and 300 V. The plasma parameters and subsequently computed quantities for every run can be found in Table 1. Figure 3 shows IEDs for conditions of 600 W RF power, 100 V bias voltage, and 10 and 60 mTorr neutral pressure, corresponding to low and high collisionality systems, respectively. The 10 mTorr case has a calculated collisionality of 0.08, while the 60

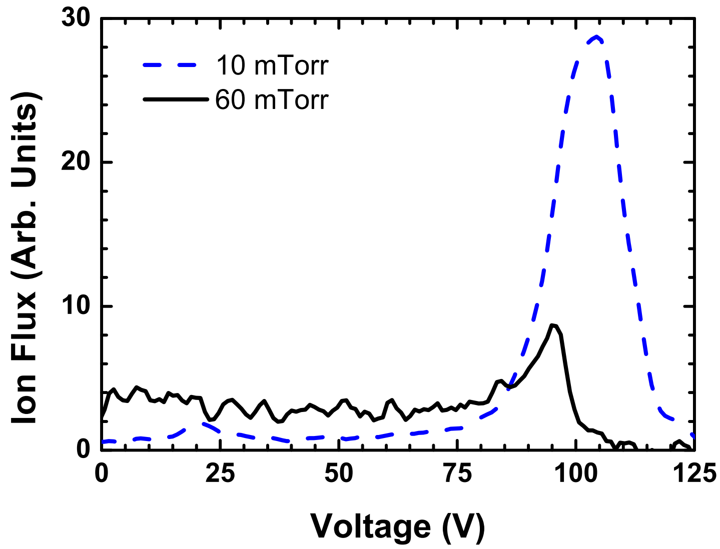

Figure 3. IEDs measured for a 100 V tailored bias waveform at 600 W RF power, and neutral pressures of 10 and 60 mTorr. The ion flux in each case has been normalized to the respective ion current density. For the 10 mTorr case, the collisionality of the system is low (0.08) and peak-to-total area ratio is 0.84. For the 60 mTorr case, the collisionality is higher (2.66) and the area ratio (0.33) is appropriately lower. The effects of the more collisional sheath are apparent in both the reduction of peak height at 100 eV and the increase of ion flux across the span of lower ion energies.

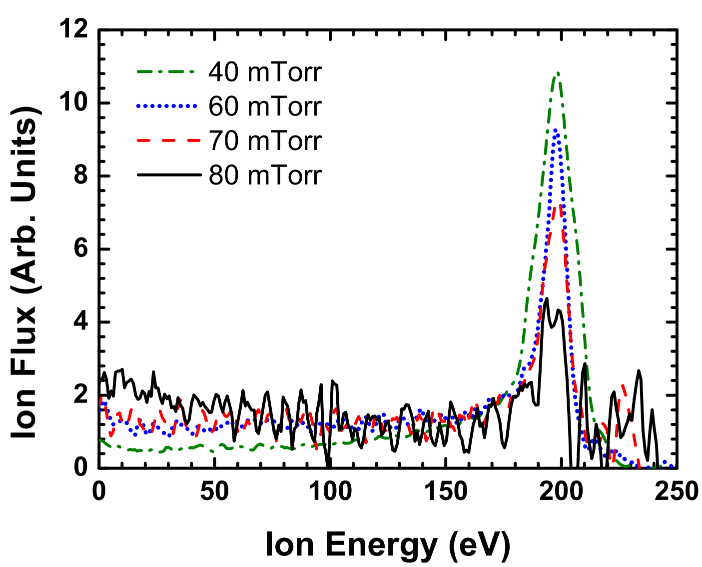

Figure 4. IEDs measured for a 200 V tailored bias waveform at 900 W RF power, and neutral pressures of 40, 60, 70, and 80 mTorr. The ion flux in each case has been normalized so all four IEDs have the same total area. As the pressure increases from 40 to 80 mTorr, the collisionality as increases: 0.51, 1.47, 1.82, and 3.41, respectively. Likewise, the area ratio decreases: 0.90, 0.38, 0.37, 0.29, respectively. The peak height clearly decreases and the lower energy ion flux increases as the system becomes more collisional.

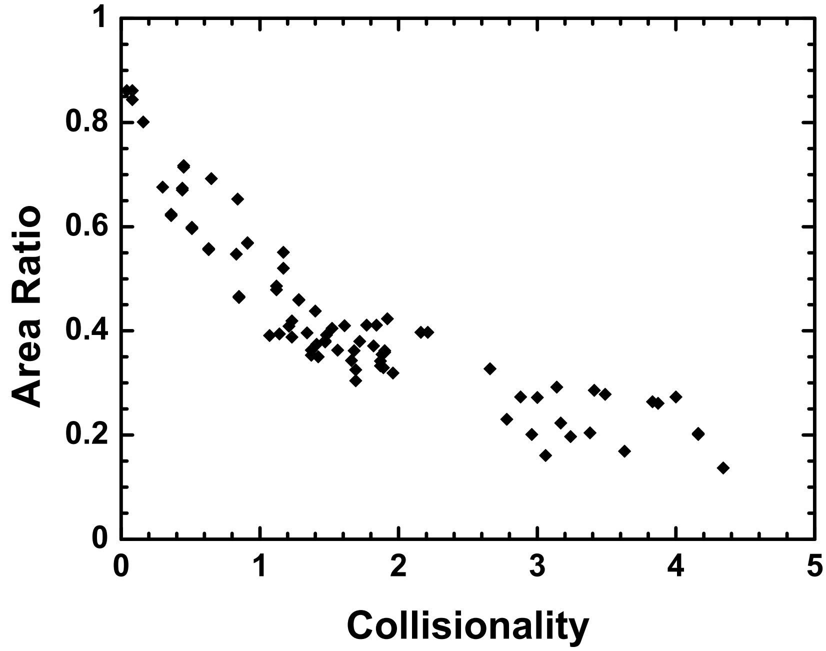

Figure 5. Area ratio versus collisionality for various system configurations including neutral pressures of 10, 40, 60, 70, and 80 mTorr, RF power levels of 300, 600, and 900 W, and tailored waveform bias voltages of 20, 100, 200, and 300 V. It can be seen that as collisionality increases, the area ratio of the IED decreases, corresponding to the peak height suppression that is expected. As more ions suffer collisions, fewer ions arrive with the full energy to be within the span of the peak.

mTorr case has a collisionality of 2.66. It is apparent that the height of the peak relative to the rest of the IED is diminished in the higher collisionality case. This corresponds to the expected peak height suppression due to incident ions losing energy to collisions while traversing the sheath. This can also be seen in Figure 4, which contains IEDs for conditions of 900 W RF power, 200 V bias voltage, and 40, 60, 70, and 80 mTorr neutral pressure. As the pressure increases, the collisionality increases and the area ratio decreases. The progressive suppression of the IED peak height and the increase in lower-energy ion flux is apparent.

For each IED measured, the collisionality and AR were calculated and the results plotted in Figure 5. For each IED the bounds of the ion energy span over which the peak area is

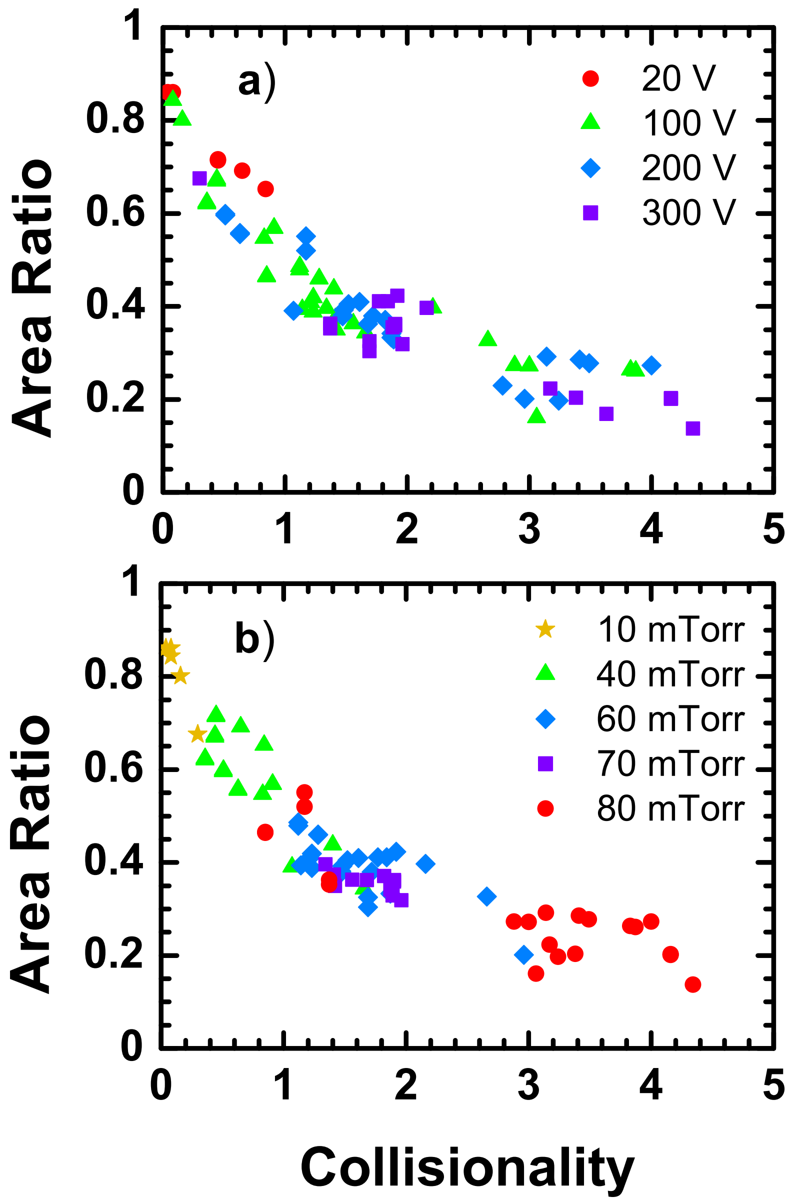

Figure 6. Area ratio versus collisionality for various system configurations, grouped by a) approximate sheath voltage and b) neutral pressure of the system. A trend of increasing collisionality with increasing neutral pressure is present, corresponding to the decreasing ion mean free path. There is some correlation of higher collisionality with higher sheath voltage, although as discussed earlier the sensitivity of the collisionality to variations in the sheath voltage is not as drastic as for variations in the neutral pressure.

integrated is determined by where the ion energy peak meets the baseline ion flux. As the collisionality of a system increases, the area ratio decreases, which is the expected behavior due to peak height suppression from collisions in the sheath. As can be seen in Figure 6a, there is a general trend of increasing collisionality with increasing neutral pressure, confirming the original strategy for achieving a highly collisional system. For zero collisionality, the data show an AR of approximately 0.85. This is consistent with the shape of the tailored bias waveform, since the periodic voltage spike comprises approximately 15 percent of the waveform period. During this portion of the cycle, the sheath potential will not be equal to the intended bias voltage, resulting in ions arriving with an energy lower than that of the peak and subsequently capping the area ratio at 0.85. For systems with high collisionality nearing 5, the AR approaches a value of 0.15. This is consistent with peak height suppression in the IED. As the sheath becomes more collisional, the peak eventually ceases to become a peak as fewer incident ions arrive with the full sheath potential. The energy span integrated over to find the peak area is approximately 15 percent of the total ion energy range. Therefore in a highly collisional system where the IED becomes a flat distribution of ion flux ranging from 0 eV to the intended bias level, the expected AR will be approximately 0.15. For even higher collisionality it is possible that no ions will arrive with the full sheath energy, eventually forcing the AR to become less than the percentage of the integration range.

One method of examining the shape of Figure 5 is to consider a prediction of the fraction of ions that should be present in the peak energy range. The ion transit time through the

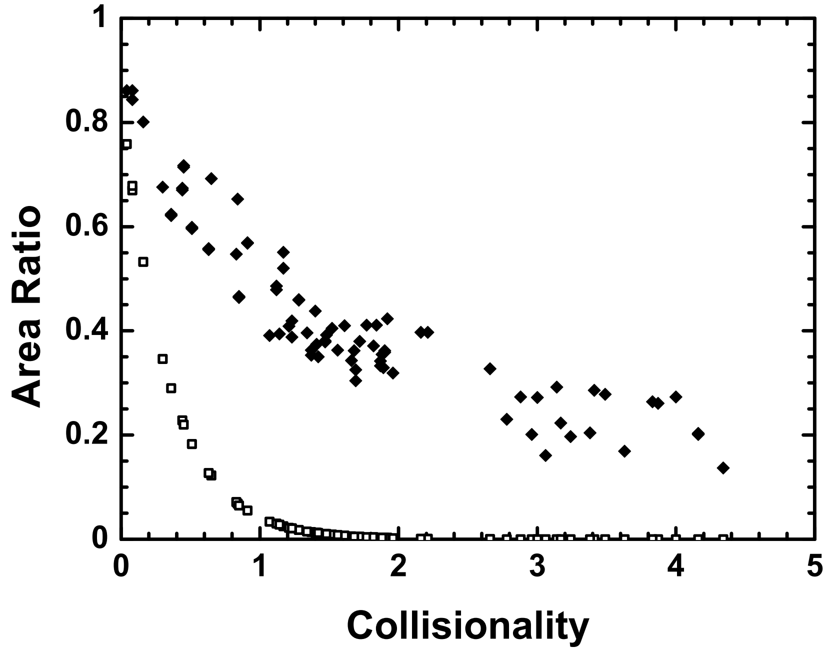

Figure 7. Measured IED area ratio (solid diamonds) versus collisionality for various system configurations including neutral pressures of 10, 40, 60, 70, and 80 mTorr, RF power levels of 300, 600, and 900 W, and tailored waveform bias voltages of 20, 100, 200, and 300 V. A prediction of the area ratio for a given collisionality (hollow squares) obeying the relation of $AR = I_0 e^{-\tau_i/\tau_{col}}$ is also plotted, but it is clear that while having similar values for very low collisionality, the exponential prediction drops off much faster than the observed data.

sheath can be calculated with[6]:

$$\tau_i = 3d_s \left(\frac{m_i}{2e\bar{V}_s}\right)^{1/2}. \tag{4}$$

The mean time between collisions of an ion moving through a sheath can also be calculated by the relation[4]:

$$\tau_{col} = \frac{\lambda_i}{v_{ion}}. \tag{5}$$

If we assume that if an ion undergoes a collision it loses sufficient energy to cause it arrive outside of the peak energy range, then given the two times above, the area ratio should be of the form $AR = I_0 e^{-\tau_i/\tau_{col}}$, where I_0 is the base fraction of incident ions experiencing acceleration through the full sheath ($\approx$ 85% due to the shape of the tailored waveform). Plotting this predicted area ratio versus collisionality in Figure 7, it is apparent that while the measured data does have the shape of an exponential decay, the area ratio does not drop off as quickly as predicted with the aforementioned calculation.

4. Conclusions

Ion energy distributions at an electrode biased with a tailored bias waveform were measured for a range of plasma conditions. The collisionality parameter C was defined as the ratio of the sheath thickness to the ion mean free path. The conditions measured included collisionalities as low as 0.05 and as high as 4.5. For collisionless sheaths (i.e. $C < 1$), the incident ions arrive at the substrate with the full bias energy and the resulting IED peak accounts for nearly all of the incident ion flux. For collisional sheaths, the incident ions will undergo charge-transfer collisions in the sheath and arrive with less than the intended bias energy, resulting in a suppression in the height of the IED peak. To quantify this peak height suppression, the area ratio parameter AR is defined to be the ratio of the peak area to the total IED area. As a system's collisionality increases, the area ratio is expected to decrease as peak suppression occurs. The IEDs measured for the various plasma conditions in this experiment support this downward trend. For very collisional systems the area of the IED peak is severely reduced, the the lower-energy ion flux increases accordingly.

References

[1] F L Buzzi, Y-H Ting, and A E Wendt. Energy distribution of bombarding ions in plasma etching of dielectrics. *Plasma Sources Science and Technology*, 18(2):025009 (8pp), 2009.

[2] A. V. Phelps. Cross Sections and Swarm Coefficients for Nitrogen Ions and Neutrals in N_2 and Argon Ions and Neutrals in Ar for Energies from 0.1 eV to 10 keV. *Journal of Physical and Chemical Reference Data*, 20:557–573, May 1991.

[3] C. Wild and P. Koidl. Ion and electron dynamics in the sheath of radio-frequency glow discharges. *Journal of Applied Physics*, 69:2909–2922, March 1991.

[4] M. A. Lieberman and A. J. Lichtenberg. *Principles of Plasma Discharges and Materials Processing.* John Wiley & Sons, second edition, 2005.

[5] D. Gahan, B. Dolinaj, and M. B. Hopkins. Retarding field analyzer for ion energy distribution measurements at a radio-frequency biased electrode. *Review of Scientific Instruments*, 79(3):033502, 2008.

[6] E. Kawamura, V. Vahedi, M. A. Lieberman, and C. K. Birdsall. Ion energy distributions in rf sheaths; review, analysis and simulation. *Plasma Sources Science and Technology*, 8(3):R45–R64, 1999.

Table 1. Plasma parameter data for each configuration measured.

Power (W)	p (mTorr)	V_{bias} (V)	V_s (V)	J_{ion} (A/m^2)	d_s (m)	σ_{CT} (m^{-2})	λ_i (m)	Collisionality	Peak Area	Area Ratio	τ_i (s)	τ_{col} (s)
300	10	20	32	3.74	6.45E-04	4.36E-19	8.12E-03	0.08	2.04E-06	0.861	1.57E-07	6.56E-07
300	10	100	107	4.45	1.46E-03	3.78E-19	9.38E-03	0.16	2.29E-06	0.801	1.94E-07	4.15E-07
300	10	300	289	5.34	2.81E-03	3.31E-19	9.39E-03	0.30	2.90E-06	0.676	2.27E-07	2.53E-07
300	40	20	21	0.31	1.63E-03	4.56E-19	1.94E-03	0.84	9.41E-08	0.653	4.88E-07	1.94E-07
300	40	20	28	1.57	9.01E-04	4.43E-19	2.00E-03	0.45	3.11E-07	0.717	2.34E-07	1.73E-07
300	40	20	28	1.57	9.01E-04	4.43E-19	2.00E-03	0.45	3.10E-07	0.714	2.34E-07	1.73E-07
300	40	100	98	0.56	3.86E-03	3.81E-19	2.32E-03	1.66	7.83E-08	0.343	5.35E-07	1.07E-07
300	40	100	103	1.98	2.13E-03	3.79E-19	2.34E-03	0.91	2.81E-07	0.569	2.88E-07	1.05E-07
300	40	100	103	1.98	2.13E-03	3.79E-19	2.34E-03	0.91	2.81E-07	0.568	2.88E-07	1.05E-07
600	10	20	32	16.38	3.08E-04	4.36E-19	8.12E-03	0.04	7.41E-06	0.861	7.48E-08	6.56E-07
600	10	100	106	18.87	7.05E-04	3.78E-19	9.37E-03	0.08	1.03E-05	0.844	9.40E-08	4.16E-07
600	40	20	23	0.59	1.27E-03	4.52E-19	1.96E-03	0.65	2.02E-07	0.692	3.62E-07	1.87E-07
600	40	100	101	0.81	3.27E-03	3.80E-19	2.33E-03	1.40	2.00E-07	0.438	4.47E-07	1.06E-07
600	40	100	96	7.83	1.02E-03	3.83E-19	2.31E-03	0.44	1.86E-06	0.674	1.42E-07	1.08E-07
600	40	100	96	7.83	1.02E-03	3.83E-19	2.31E-03	0.44	1.81E-06	0.670	1.42E-07	1.08E-07
600	40	200	191	8.81	1.61E-03	3.50E-19	2.53E-03	0.63	1.85E-06	0.556	1.59E-07	8.37E-08
600	40	200	191	8.81	1.61E-03	3.50E-19	2.53E-03	0.63	1.88E-06	0.558	1.59E-07	8.37E-08
600	60	100	94	0.47	4.10E-03	3.84E-19	1.54E-03	2.66	5.56E-08	0.327	5.80E-07	7.25E-08
600	60	100	98	2.12	1.98E-03	3.81E-19	1.55E-03	1.28	2.89E-07	0.459	2.75E-07	7.15E-08
600	60	100	98	2.12	1.98E-03	3.81E-19	1.55E-03	1.28	3.02E-07	0.460	2.75E-07	7.15E-08
600	60	100	100	2.37	1.91E-03	3.80E-19	1.55E-03	1.23	3.05E-07	0.419	2.61E-07	7.10E-08
600	60	100	100	2.42	1.89E-03	3.80E-19	1.55E-03	1.21	2.90E-07	0.409	2.59E-07	7.10E-08
600	60	200	191	0.91	4.99E-03	3.50E-19	1.69E-03	2.96	6.55E-08	0.201	4.95E-07	5.58E-08
600	60	200	190	2.27	3.15E-03	3.50E-19	1.69E-03	1.87	2.83E-07	0.333	3.13E-07	5.59E-08
600	60	200	190	2.27	3.15E-03	3.50E-19	1.69E-03	1.87	2.90E-07	0.333	3.13E-07	5.59E-08
600	60	200	194	3.51	2.57E-03	3.49E-19	1.69E-03	1.52	4.33E-07	0.405	2.54E-07	5.55E-08
600	60	200	197	3.22	2.72E-03	3.49E-19	1.69E-03	1.61	3.93E-07	0.410	2.66E-07	5.51E-08
600	60	300	285	0.99	6.46E-03	3.32E-19	1.78E-03	3.63	8.01E-08	0.169	5.25E-07	4.82E-08
600	60	300	287	4.63	3.01E-03	3.31E-19	1.78E-03	1.69	3.56E-07	0.304	2.43E-07	4.81E-08
600	60	300	287	4.63	3.01E-03	3.31E-19	1.78E-03	1.69	3.71E-07	0.325	2.43E-07	4.81E-08
600	60	300	287	3.58	3.42E-03	3.31E-19	1.78E-03	1.92	4.23E-07	0.423	2.77E-07	4.81E-08
600	60	300	289	2.83	3.86E-03	3.31E-19	1.78E-03	2.16	3.47E-07	0.397	3.12E-07	4.80E-08
600	70	100	97	2.37	1.86E-03	3.82E-19	1.32E-03	1.41	2.59E-07	0.374	2.59E-07	6.15E-08
600	70	100	98	1.96	2.06E-03	3.81E-19	1.33E-03	1.56	2.06E-07	0.363	2.86E-07	6.13E-08
600	70	200	190	3.80	2.43E-03	3.50E-19	1.44E-03	1.68	3.62E-07	0.362	2.42E-07	4.79E-08
600	70	200	189	3.01	2.73E-03	3.51E-19	1.44E-03	1.89	2.65E-07	0.329	2.72E-07	4.80E-08
600	70	300	283	4.90	2.89E-03	3.32E-19	1.52E-03	1.90	3.80E-07	0.362	2.36E-07	4.14E-08
600	70	300	283	4.90	2.89E-03	3.32E-19	1.52E-03	1.90	3.63E-07	0.359	2.36E-07	4.14E-08
600	80	100	96	0.65	3.54E-03	3.83E-19	1.16E-03	3.06	1.02E-08	0.161	4.96E-07	5.40E-08
600	80	100	96	0.40	4.47E-03	3.83E-19	1.16E-03	3.87	4.44E-08	0.261	6.26E-07	5.40E-08
600	80	100	97	0.42	4.43E-03	3.82E-19	1.16E-03	3.83	4.65E-08	0.264	6.18E-07	5.38E-08
600	80	200	190	1.34	4.10E-03	3.50E-19	1.26E-03	3.24	3.86E-08	0.197	4.08E-07	4.19E-08
600	80	200	192	0.89	5.06E-03	3.50E-19	1.27E-03	4.00	7.48E-08	0.273	5.01E-07	4.18E-08
600	80	200	193	1.18	4.42E-03	3.50E-19	1.27E-03	3.49	7.36E-08	0.278	4.37E-07	4.17E-08
600	80	300	290	1.25	5.82E-03	3.31E-19	1.34E-03	4.34	6.98E-08	0.137	4.69E-07	3.60E-08
600	80	300	286	1.35	5.56E-03	3.31E-19	1.34E-03	4.16	6.44E-08	0.203	4.51E-07	3.61E-08
600	80	300	284	1.34	5.55E-03	3.32E-19	1.33E-03	4.16	7.37E-08	0.201	4.52E-07	3.62E-08

Table 1. (Continued)

Power (W)	p (mTorr)	V_{bias} (V)	V_s (V)	J_{ion} (A/m^2)	d_s (m)	σ_{CT} (m^{-2})	λ_i (m)	Collisionality	Peak Area	Area Ratio	τ_i (s)	τ_{col} (s)
900	40	100	96	2.22	1.91E-03	3.83E-19	2.31E-03	0.83	5.96E-07	0.547	2.68E-07	1.08E-07
900	40	100	99	12.15	8.35E-04	3.81E-19	2.33E-03	0.36	2.51E-06	0.621	1.15E-07	1.07E-07
900	40	100	99	12.15	8.35E-04	3.81E-19	2.33E-03	0.36	2.54E-06	0.624	1.15E-07	1.07E-07
900	40	200	191	3.07	2.72E-03	3.50E-19	2.53E-03	1.07	5.90E-07	0.391	2.70E-07	8.37E-08
900	40	200	189	13.39	1.29E-03	3.51E-19	2.53E-03	0.51	2.98E-06	0.596	1.29E-07	8.40E-08
900	40	200	189	13.39	1.29E-03	3.51E-19	2.53E-03	0.51	3.00E-06	0.599	1.29E-07	8.40E-08
900	60	100	95	0.69	3.40E-03	3.83E-19	1.54E-03	2.21	1.17E-07	0.397	4.78E-07	7.22E-08
900	60	100	95	2.70	1.72E-03	3.83E-19	1.54E-03	1.12	4.24E-07	0.486	2.42E-07	7.22E-08
900	60	100	95	2.70	1.72E-03	3.83E-19	1.54E-03	1.12	4.32E-07	0.479	2.42E-07	7.22E-08
900	60	100	97	2.27	1.90E-03	3.82E-19	1.55E-03	1.23	2.74E-07	0.388	2.65E-07	7.17E-08
900	60	100	96	2.61	1.76E-03	3.83E-19	1.54E-03	1.14	3.01E-07	0.394	2.46E-07	7.20E-08
900	60	200	191	1.04	4.68E-03	3.50E-19	1.69E-03	2.78	1.11E-07	0.230	4.64E-07	5.58E-08
900	60	200	190	3.68	2.47E-03	3.50E-19	1.69E-03	1.47	4.49E-07	0.381	2.46E-07	5.59E-08
900	60	200	190	3.68	2.47E-03	3.50E-19	1.69E-03	1.47	4.55E-07	0.379	2.46E-07	5.59E-08
900	60	200	191	2.69	2.90E-03	3.50E-19	1.69E-03	1.72	3.11E-07	0.380	2.88E-07	5.58E-08
900	60	200	191	3.63	2.50E-03	3.50E-19	1.69E-03	1.48	3.65E-07	0.392	2.48E-07	5.58E-08
900	60	300	285	3.84	3.28E-03	3.32E-19	1.78E-03	1.84	3.83E-07	0.411	2.67E-07	4.82E-08
900	60	300	282	4.12	3.15E-03	3.32E-19	1.78E-03	1.77	4.19E-07	0.411	2.57E-07	4.84E-08
900	70	100	96	2.58	1.77E-03	3.83E-19	1.32E-03	1.34	3.31E-07	0.396	2.48E-07	6.17E-08
900	70	100	95	2.27	1.87E-03	3.83E-19	1.32E-03	1.42	2.53E-07	0.350	2.64E-07	6.19E-08
900	70	200	191	3.27	2.63E-03	3.50E-19	1.45E-03	1.82	3.27E-07	0.371	2.62E-07	4.78E-08
900	70	200	189	3.08	2.69E-03	3.51E-19	1.44E-03	1.87	2.88E-07	0.342	2.69E-07	4.80E-08
900	70	300	284	4.98	2.87E-03	3.32E-19	1.53E-03	1.88	3.59E-07	0.355	2.34E-07	4.14E-08
900	70	300	284	4.58	3.00E-03	3.32E-19	1.53E-03	1.96	2.87E-07	0.319	2.44E-07	4.14E-08
900	80	100	102	8.90	9.98E-04	3.79E-19	1.17E-03	0.85	1.16E-06	0.464	1.36E-07	5.28E-08
900	80	100	102	8.90	9.98E-04	3.79E-19	1.17E-03	0.85	1.16E-06	0.466	1.36E-07	5.28E-08
900	80	100	96	0.73	3.33E-03	3.83E-19	1.16E-03	2.88	5.65E-08	0.273	4.66E-07	5.40E-08
900	80	100	97	0.68	3.47E-03	3.82E-19	1.16E-03	3.00	6.17E-08	0.272	4.84E-07	5.38E-08
900	80	200	196	10.64	1.49E-03	3.49E-19	1.27E-03	1.17	1.58E-06	0.551	1.46E-07	4.14E-08
900	80	200	196	10.64	1.49E-03	3.49E-19	1.27E-03	1.17	1.58E-06	0.520	1.46E-07	4.14E-08
900	80	200	192	1.23	4.32E-03	3.50E-19	1.27E-03	3.41	8.45E-08	0.286	4.27E-07	4.18E-08
900	80	200	194	1.46	3.98E-03	3.49E-19	1.27E-03	3.14	8.53E-08	0.292	3.92E-07	4.16E-08
900	80	300	284	12.37	1.82E-03	3.32E-19	1.33E-03	1.37	1.18E-06	0.363	1.48E-07	3.62E-08
900	80	300	284	12.37	1.82E-03	3.32E-19	1.33E-03	1.37	1.19E-06	0.353	1.48E-07	3.62E-08
900	80	300	283	2.28	4.24E-03	3.32E-19	1.33E-03	3.17	1.04E-07	0.223	3.45E-07	3.63E-08
900	80	300	285	2.02	4.52E-03	3.32E-19	1.34E-03	3.38	8.10E-08	0.204	3.67E-07	3.62E-08